
Paleoenvironmental implications of Deccan volcanism relative to the Cretaceous-Paleogene mass extinction: evidence from the 'red bole' record

Nikhil Sharma[1,2], Thierry Adatte[2], Torsten Vennemann[3], Blair Schoene[4], Gerta Keller[4], Syed F. R. Khadri[5]

[1]Department of Earth Sciences, University of Geneva, Rue des Maraichers 13, 1205 Geneva, Switzerland

[2]Institute of Earth Sciences (ISTE), University of Lausanne, 1015 Lausanne, Switzerland

[3]Institute of Earth Surface Dynamics (IDYST), University of Lausanne, 1015 Lausanne, Switzerland

[4]Department of Geosciences, Princeton University, Princeton, NJ 08544, USA

[5]P.G. Department of Geology, Amravati University, Amravati 222602, Maharashtra, India

Corresponding author: Nikhil Sharma (nikhil.sharma@unige.ch)

Abstract

Large Igneous Provinces (LIPs) have been widely studied over the past decades due to their likely link to mass extinction events. Previous work involving U-Pb zircon dating of the Deccan lava flows indicates that the main phase-2 began 250 Ka before the Cretaceous-Paleogene (K-Pg) mass extinction boundary and continued into the early Danian, suggesting a cause-and-

effect relationship. Closer to the eruption centre, intra-volcanic red weathered horizons known as red boles mark quiescent periods between basalt flows. Red boles have increasingly attracted the attention of researchers to understand the prevailing climatic conditions during the Deccan volcanic activity for their ability to yield crucial evidence of environmental changes triggered by volcanic activity using different geochemical proxies such as major elemental composition, bulk rock and clay mineralogy, weathering indices, paleo-precipitation estimates and stable isotope analysis. Our results indicate that red boles are characterized by concentrations of immobile elements such as Al and Fe^{3+} ions that are typical of paleo-laterites, which develop over short periods of weathering. Identified clay minerals consist mostly of smectite indicative of semi-arid monsoonal conditions. Weathering indices suggest intense weathering most likely linked to increasing acid rains while stable H- and O-isotope compositions suggest increasing paleoclimate instability in parallel to increased eruption rates just before the K-Pg boundary. The multi proxy approach is compatible with a cause-and-effect relationship between the Deccan Trap eruptions and the K-Pg mass extinction.

Keywords: LIPs, Deccan volcanism, K-Pg boundary, Paleoclimate, red boles, geochemistry

1. Introduction

The cause of the Cretaceous-Paleogene (K-Pg) mass extinction is often attributed to an extra-terrestrial impact supported by evidence such as a global iridium enrichment layer (Alvarez et al., 1980), impact spherule ejecta in Mexico and Central America (e.g., Smit et al., 1996; Schulte et al., 2010; Pope et al., 1991) and the discovery of the Chicxulub impact crater on the Yucatan peninsula, in Mexico (Hildebrand et al., 1991). However, subsequent research has focussed more on Large Igneous Provinces (LIPs) and the possibility of a cause-and-effect relationship between LIPs and mass extinctions events. The relationship between the two

strengthened considerably after the discovery of a close link between the two phenomena (e.g., Wignall, 2001; Rampino and Stothers, 1988; Olsen, 1999; Sepkoski, 1982, 1996). Deccan volcanism, therefore, rapidly became an alternative cause of the K-Pg mass extinction (e.g., McLean, 1985; Courtillot et al., 1986, 1988; Duncan and Pyle, 1988; Wignall, 2001; Officer and Drake, 1983).

The Deccan Volcanic Province (DVP) is situated in Western India and covers an area of about 500,000 km^2 (Widdowson et al., 1997). It is one of the most important Large Igneous Provinces (LIPs) and consists of the world's longest lava flow ever recorded (>1500 km into the Krishna Godavari Basin in the Gulf of Bengal in Eastern India) (Keller et al., 2011; Self et al., 2008). Recent studies have revealed that the eruptions took place in three major phases: phase-1 in C30n, the main phase-2 in C29r and the final phase-3 in C29n. Phase-2 was the most important as it accounts for 80 % of the total 3500 m thick lava pile and erupted in pulses over a short period of time in C29r just before the mass extinction (Chenet et al., 2008). U-Pb zircon geochronology (Schoene et al., 2015) also suggests that the main phase-2 erupted over 750 Ka in magnetic polarity C29r and began 250 Ka before the K-Pg extinction event and continued for 500 Ka into the early Danian, suggesting a cause-and-effect relationship. Latest U-Pb geochronology (Schoene et al., 2019; Eddy et al., 2020) suggests that the K-Pg boundary is located at the top of Poladpur Formation (Fm) (66.016 ± 0.050 Ma), about 70 Ka after an acceleration in the eruption rate.

The main goal of this paper is to study the paleoenvironmental changes linked to Deccan volcanism using detailed mineralogical and geochemical analysis of 26 red bole sections (Fig. 1). Red boles, also known as 'Bole Beds', are weathered horizons formed from the weathering of basalts during periods of volcanic inactivity (e.g., Widdowson et al., 1997, Gosh et al 2006). Red boles show a characteristic lithological succession and are laterally continuous, but with laterally variable thickness. This study examines the major elemental composition using X-ray

fluorescence (XRF), bulk-rock, and clay mineralogy using X-ray diffraction (XRD), estimates of weathering indices such as the chemical index of alteration (CIA), the index of lateritisation (IOL), the chemical index of weathering (CIW) along with estimates of Mean Annual Precipitation (MAP) for the red boles. Stable isotope (hydrogen and oxygen) compositions of an isolated clay fraction are also studied. These results provide an overview of the conditions of weathering and the paleoclimatic conditions during the Deccan volcanic activity and the results are discussed in the context of the K-Pg mass extinction.

2. Geological Background

The Deccan Volcanic Province (DVP), located in the western peninsular of India (Fig. 1) (Babechuk et al., 2014), is one of the largest flood basalt provinces on Earth and currently covers an area of approximately 500,000 km^2, with an original extent that was probably more than 1,500,000 km^2 (Fig. 1) (Widdowson et al., 1997). Hundreds of lava flows reached a total thickness of approximately 3000 m near the eruptive center (Beane et al., 1986; Cox and Hawkesworth 1985; Khadri et al.,1988) and flowed eastward with a total volume greater than 1.3 million km^2 (Jay and Widdowson 2008).

Individual lava flows can be easily identified and based on a detailed geochemical analysis, the Deccan basalt group has been stratigraphically divided into three subgroups and ten formations (Beane et al., 1986). The entire stratigraphic sequence is approximately 3600 m thick and is exposed from north to south along the full length of the Western Ghats. The Kalsubai Subgroup is the lowermost subgroup and consists of the lower five formations (Fm), i.e., Jawar, Igatpuri, Neral, Thakurvadi and Bhimashankar, from bottom to top (Fig.2D). The Kalsubai subgroup is overlain by the Lonavala subgroup, which includes two Fm, the Khandala and Bushe Fm (Fig.2D). The Wai Subgroup lies above the Khandala Subgroup and consists of the Poladpur, Ambenali, Mahabaleshwar and Panhala Fm (Fig. 2D).

A particular feature of the Deccan Traps is the presence of so-called 'red boles' or 'bole horizons', which are weathered horizons occurring at the top of lava flows and are indicative of periods of volcanic quiescence. They are easily identifiable in the field by their distinctive red colour, although they can also be found in a range of colours from red through to brown along with green boles (Widdowson et al., 1997). Red boles (Fig.2B, 2C) show a characteristic lithological succession, which starts with fresh underlying basalt and grades through different weathering phases such as weathered amygdaloidal basalt, friable red clay, and occasionally red clay paleosol, which is overlain by the next basalt flow (Fig.2B, 2C; Fig. 3). Deccan phase-2 includes at least fifty exposed red bole layers with many still potentially undiscovered. Bole beds are commonly considered to be the result of in-situ alteration of flow tops resulting in a fossilized profile reflecting weathering effects which occurred at the time of eruptions (Widdowson et al., 1997) and are usually formed over a period <100 Kyr. Red boles are thus crucial to interpret the paleoclimatic conditions that prevailed during the Deccan eruptions and its impact on the K-Pg boundary mass extinction.

3. Methods

3.1 Sample preparation

Samples (N = 167) were prepared for analysis at the University of Lausanne, Switzerland. Samples were first dried at 45 °C for 2–3 days to remove humidity. Dried samples were then crushed and powdered using an agate mill.

3.2 Major elemental composition (XRF)

Major elements were analysed on fused beads using the PANalytical Axios-mAX spectrometre with a Rh anode radiation and power of 4 kW at the Earth Science Institute of the University of Lausanne, Switzerland. First, 2–2.5 g of rock powder was calcinated over 3h at 1050°C to remove any volatiles present. Loss on Ignition (LOI) was calculated using Equation 1.

$$\mathrm{LOI} = \left(\frac{W}{W_i} \times 100\right) - 100 \quad (1)$$

where W_i and W are the weights before and after calcination respectively. Next, 6.0000 ± 0.0002 g of LithiumTetraborate ($Li_2B_4O_7$) were added to 1.2000 ± 0.0002 g of calcinated powder and mixed for 3 minutes to obtain a homogeneous mixture. Fused beads were then prepared by using the PANalytical Perl'X 3 by heating the mixture at 1250°C.

3.3 Bulk rock and clay mineralogy (XRD)

Bulk rock and clay mineralogy was analyzed at the Institute of Earth Sciences of the University of Lausanne, Switzerland (Thermo Scientific ARL X-TRA Diffractometer) using the procedure described by Klug and Alexander (1974), Kübler (1983) and Adatte et al. (1996). Bulk rock mineralogy was analyzed on powdered samples pressed into powder holders. Clay minerals were analyzed for the <2 μm fraction. Carbonates were removed with HCl (10 %), and the insoluble residue was washed and centrifuged until a neutral suspension was obtained. Following the Stokes law, the granulometric fraction <2 μm was pipetted and deposited on a glass plate and air-dried. Analyses by X-ray diffraction of oriented clay samples were performed after air-drying and ethylene-glycol solvation. The intensities of the identified clay mineral were measured in counts (cps) and an estimation of the proportion of clay minerals is given in relative per cent (%).

3.4 Weathering indices

To quantify the extent of weathering and obtain a weathering trend across the stratigraphic profile of the Deccan traps, weathering indices such as the chemical index of alteration (CIA), index of lateritisation (IOL), and chemical index of weathering (CIW) were used. CIA was calculated using Equation 2 as proposed by (Nesbitt and Young, 1982) using molecular proportions. Conversions into mole were done using the conversion factors given in Babechuk et al. (2014). CIA values represent changes in the feldspar and clay content such that higher CIA values reflect more intense weathering (Nesbitt and Young, 1982).

$$\mathrm{CIA} = \frac{\mathrm{Al_2O_3}}{\mathrm{Al_2O_3} + \mathrm{CaO^*} + \mathrm{Na_2O} + \mathrm{K_2O}} \times 100 \quad (2)$$

where CaO^* is the CaO incorporated in the silicate fraction.

The index of lateritisation (IOL) is an additional weathering index proposed by Babechuk et al., (2014) to overcome the inability of the CIA to quantify the advanced stages of chemical weathering. It uses the weight per cent (wt.%) of SiO_2, $Fe_2O_{3(T)}$ and Al_2O_3 as shown in Equation 3 such that higher IOL values correspond to more intense weathering.

$$\mathrm{IOL} = \frac{\mathrm{Al_2O_3} + \mathrm{Fe_2O_{3(T)}}}{\mathrm{Al_2O_3} + \mathrm{Fe_2O_{3(T)}} + \mathrm{SiO_2}} \times 100 \quad (3)$$

The chemical index of weathering (CIW) (Eq. 4), proposed by (Harnois, 1988), has an approach similar to the CIA. CIW excludes the inconsistent behaviour of Potassium (K) during pedogenesis (Sheldon and Tabor, 2009) and is an improved index to measure weathering relative to the source rock. (Harnois, 1988). An increase in CIW values indicates an increase in weathering.

$$\mathrm{CIW} = \frac{\mathrm{Al_2O_3}}{\mathrm{Al_2O_3} + \mathrm{CaO^*} + \mathrm{Na_2O}} \times 100 \quad (4)$$

3.5 Mean Annual Precipitation

Mean annual precipitation (MAP) was reconstructed using the CIW (Eq. 5; standard error = ± 182 mm yr^{-1}) (Sheldon et al., 2002; Stein et al., 2021) as:

$$\mathrm{MAP(mm\ /\ yr)} = 221.1e^{0.0197(\mathrm{CIW})} \quad (5)$$

3.6 Stable isotope analysis (hydrogen and oxygen)

Stable isotope compositions were analysed for a group of selected samples that contain smectite and only small amounts of hematite, quartz, and goethite.

3.6.1 Oxygen isotope analysis

Samples were analysed for $\delta^{18}O$ values using the laser fluorination line of the stable isotope laboratory of the University of Lausanne, Switzerland. Oxygen gas is extracted based on a method by Sharp (1990) and outlined in Vennemann et al., (2001). Samples were mixed and homogenized with barium fluoride powder as described in Kirschner and Sharp (1997) to reduce the sputtering of the samples. About 2 mg of samples are weighed into a platinum holder and placed in a reaction chamber which is evacuated to 10^{-6} mbar and pre-fluorinated for 48 h to remove any adsorbed water molecules. After repeated pre-fluorination before the analysis run, samples were heated using a CO_2 laser with an IR wavelength of 10.6 µm in an atmosphere of 50 mbar of F_2 gas. After the reaction, the sample gas is transferred where F_2 is removed by reaction with heated KCl salt, and the pure oxygen gas is expanded into a Thermo Finnigan MAT 253 isotope ratio mass spectrometer. An in-house quartz standard (LS-1) was analysed during every run and the results were normalized to its accepted value of +18.1‰.

3.6.2 Hydrogen isotope analysis (δD)

Hydrogen isotope compositions were measured at the University of Lausanne, Switzerland. Samples were prepared as described in (Bauer and Vennemann, 2014; Bauer et al., 2016). About 2 mg of sample is weighed in silver capsules of size 3.3 × 5 mm. Adsorbed water was removed by heating the samples to 250 °C for 3 hours while pumping to vacuum. Samples were then stored in evacuated glass tubes until analysis. Few samples were loaded at a time into a He-flushed zero-blank auto sampler to reduce rehydration. They were then heated to 1450°C and H_2 was separated from CO_2, N_2 in a gas chromatograph and analysed for its D/H ratio with a Thermo Finnigan Delta Plus XL mass spectrometer. Values were normalized using a kaolinite standard, K-17 (-125 ‰, 14.5 wt.% H_2O) and a biotite standard, G1 (-66 ‰, 3.3 wt.% H_2O) were used.

Results for both $\delta^{18}O$ and δD values are reported relative to VSMOW (Vienna Standard Mean Ocean Water) in delta-notation with a value of 0 ‰ for VSMOW and -55.5 ‰ (oxygen)/ -

428‰ (hydrogen) for SLAP (Standard Light Antarctic Precipitation) (Coplen, 1996; Bauer et al., 2016).

4. Results and Interpretation

4.1 Lithological description of a typical red bole

A typical red bole, such as Red Bole DJ (section RBDJ) (Fig. 3), sampled in the upper Mahabaleshwar Fm at an elevation of 608 m. RBDJ begins with weathered basalt at the base of the section followed by a thick red bole (1.20 m) with red clays on top (0.3 m), overlain by weathered basalt. Results are first provided for section RBDJ to document geochemical changes within a typical red bole, followed by the average result from each studied red bole relative to the Deccan basalt group.

4.2 Bulk rock and clay mineralogy of section RBDJ

Phyllosilicates constitute a major part of RBDJ with up to 86 % in the red clays. Bulk rock mineralogy of section RBDJ is given in Fig. 4. Quartz is absent throughout the section except in sample RBDJ – 5 (red clays) where 4 % of quartz is present and must be likely of aeolian origin. Ca-rich plagioclase (Labradorite) is present throughout the section with a maximum value of 21 % in sample RBDJ – 7 (upper weathered basalt) while the average amount is lower in the rest of the section (2.5 %). Hematite contents reach a peak of 16 % in the red bole sample RBDJ – 3 followed by a decrease towards the top of the section. Goethite values are constant within the section with an average value of 4 %. Clay mineralogy of red boles consists almost entirely of smectite along with trace amounts of zeolite and mica (supplementary material, Figure S1).

4.3 Major elemental composition of section RBDJ

Major elemental compositions given at weight % oxides of a typical red bole section predominantly consists of SiO_2, Al_2O_3, Fe_2O_3, CaO, and MgO. The plots of major elements for section RBDJ are displayed in Fig. 5. Average values for SiO_2, Al_2O_3 and Fe_2O_3 are 43.17

%, 13.02 % and 18.20 % respectively. SiO_2 contents are quite constant throughout the section and shows a maximum value 47.81 % in sample RBDJ-7 (weathered basalt) and a minimum value of 39.13 % in red bole sample RBDJ-2 (lower red bole). Al_2O_3 values vary from a minimum value (11.16) in sample RBDJ-5 (red clays) to a maximum value of 15.06 % in sample RBDJ-2. Fe_2O_3 amounts also show a slight variation from a minimum value of 15.53 % in sample RBDJ-7 (weathered basalt) to a maximum value (20.01 %) in sample RBDJ-4 (top red bole). TiO_2 is characterized by an average value of 3.57 %. Mobile elements, for example Ca (linked to Ca from plagioclase) expressed as CaO, MgO, Na_2O and K_2O have average concentrations of 3.03 %, 3.17 %, 0.43 % and 0.22 %, respectively. Loss on Ignition (LOI) range from 2.9 % (sample RBDJ-7, weathered basalt) to 17.7 % (sample RBDJ-5, red clays). Such LOI values are comparable to those found by Font et al., (2020) in other red bole sections.

4.4 Weathering indices and MAP from section RBDJ

CIA values for section RBDJ are given in Fig. 6A and increase from the basal weathered basalt unit (RBDJ-1) from 65.2 % to a maximum value of 82.1 % in red bole sample RBDJ-4. Red clays (samples RBDJ-5 and 6) display an average value of 77 %. The minimum CIA value occurs in sample RBDJ-7 (weathered basalt) with value of 37.5 %.

The average IOL value observed in the section is 25.2 % . IOL values for section RBDJ are given in Fig. 6B. A maximum IOL value of 29.4 % is detected in sample RBDJ-2, weathered basalt). while sample RBDJ-7 (upper weathered basalt) show a minimum value of 22.1 %. Red clay samples RBDJ-5 and 6 have values of 22.9 % and 23.0 %. These values are however lower than the ones estimated by Font et al., (2020) which fluctuate between 37 % and 47 %.

CIW and MAP values increase from RBDJ-1 (weathered basalt) to RBDJ-4 (top red bole) followed by a subsequent decrease towards the top of the section (sample RBDJ-7) (Fig. 7A,

7B). Sample RBDJ-4 shows a maximum value of 82.4 % and 1121 mm/yr respectively while RBDJ-7 has the minimum value of 38.4 % and 471 mm/yr respectively.

4.5 Red bole mineralogy and major elements relative to the Deccan basalt pile

Bulk rock mineralogy of red boles consists of phyllosilicates, iron oxides including hematite and goethite, together with minor amounts of plagioclase and traces of quartz (<1 %). Clay fraction mineralogy of red boles is dominated by smectite and only small amounts of zeolite, kaolinite, and illite. The dominance of smectite indicates a semi-arid, subtropical, and seasonally variable climate during Deccan volcanism.

Major element analysis suggests that red boles are enriched in Al, Fe, and Ti, while more mobile elements such as K, Na, Ca, Mg and Si are increasingly leached towards the top of Deccan phase-2 volcanism (Fig. 11).

4.6 Weathering trends across the Deccan basalt group

CIA values indicate an overall increasing trend (increase in chemical weathering) towards the top of Deccan volcanism phase-2 from minimum average value of 40.8 % to a maximum value of 86.2 % in the Mahabaleshwar formation. CIA values for most sections are within the range of 50 – 70 % with an average value of 59.7 % (Fig. 11). Note also that the highest fluctuations in CIA values are recorded in the uppermost Ambenali and Mahabaleshwhar Fm.

The loss on ignition (LOI) accounts for the number of volatile substances present in a sample and is proportional to the amount of hydrated minerals present in addition to carbonate, organic carbon, or sulphur (Babechuk et al., 2014). During weathering, anhydrous minerals are replaced by hydrous minerals such as smectite, kaolinite, resulting in an increase in the LOI. LOI can therefore be a useful parameter in assessing the degree of weathering by providing insights into the pedogenic mineral transformations. Figure 8A shows a strong correlation between the LOI and CIA. The highly weathered samples do not plot on the correlation and

are also less hydrated. The correlation indicates a transformation of anhydrous magmatic minerals (e.g., pyroxene and plagioclase) into hydrous phyllosilicates such as smectite.

By comparison to the LOI, as the IOL increases there is a decrease in the LOI as the phyllosilicates are altered to sesquioxide of Al and Fe along with a loss of Si (Fig. 8B). The index of lateritisation (IOL) of red bole typically has a range between 30 % and 40 % with a maximum value of 65 % and minimum of 31 % suggesting an intermediate intensity of weathering (Fig. 11).

The CIW and MAP are well correlated. CIW values vary from a minimum of 35.3 % to a maximum of 86.3 %, while precipitation is calculated estimated to be between 443 to 1209 (mm yr^{-1}) (Fig. 11). Higher MAP values coincide with the increase in eruption rate at the top of the Bushe formation during the Deccan paroxysmal phases, which correspond to the Poladpur, Ambenali and Mahabaleshwhar Fm.

4.7 Implications of weathering indices as paleoclimatic proxies relative to the tempo, timing, and rate of volcanic emissions from the Deccan traps

The Chemical Index of Alteration (CIA) is a measure of the intensity of weathering with higher CIA values indicating increased chemical weathering. CIA values are better understood through the A-CN-K ternary diagram in which the 'A' apex is Al_2O_3, the 'CN' apex is $CaO+Na_2O$ and the 'K' apex represents K_2O (Fig. 9A). It can be observed that CIA values of most red bole sections are within the range of 40 to 60 % and follow a weathering trend away from the 'CN' apex, indicating a net Ca and Na removal. A complete removal would imply that the red bole has reached the kaolinitisation stage (apex A), which is however not the case. This can also be observed through the SAF ternary diagram accompanying the Index of Lateritisation (IOL) in which the 'S' apex is SiO_2, 'A' apex is Al_2O_3, and 'F' apex represents Fe_2O_3 (Fig. 9B). The IOL and the SAF plot together distinguish between the various stages of lateritisation, i.e., kaolinitised, weakly lateritised, moderately lateritised and strongly lateritised

(Fig. 9B). It can be observed that red bole sections have IOL values below 50 % indicating that they are at the very nascent stages of kaolinitisation, which is confirmed by the low abundance of kaolinite in the samples.

An increasing trend in CIA and LOI values, which reflect pedogenic mineralogical transformations (magmatic minerals into hydrous phyllosilicates and smectites), suggests an intensification of chemical weathering during the Deccan paroxysmal phases (Fig. 11). This increasing trend is consistent with accelerated weathering due to increased acid rains, which may explain the absence of root traces and organic matter in bole-beds along with the partial leaching of more resistant minerals such as silica and other mobile elements. The rate of basaltic eruptions was also not constant as it can be noted from Fig. 11. The Poladpur, Ambenali and Mahabaleshwar Fm accumulated in the upper part of Deccan pile correspond to 80 % of the volume emitted (Schoene et al., 2019). This acceleration in the rate of emissions is consistent with intensified weathering and existence of complex and extreme climatic conditions about 70 Ka before the K-Pg boundary.

4.8 Implications of stable isotope compositions to the timing and rate of volcanic emissions from the Deccan

δD values have a range for the red bole sections from -115 to -59 ‰ with an average value of -88.3 ‰. Modern soil samples (soil 20/1/16-3 and soil 30/1/17-4) have values of -77 and -84 ‰, respectively. $\delta^{18}O$ values for the clay fraction separated from the red boles have a range from 11.7 to 22 ‰ with an average of 18.3 ‰ (samples routinely reproduce to within 0.2 to 0.5 ‰). Modern soil samples have values of 17.5 ‰ (soil 20/1/16-3) and 20.4 ‰ (soil 30/1/17-4). Water content in red bole samples average at 5.08 wt.% but are 6.65 wt.% for the modern soil samples, indicating an efficient removal of adsorbed water prior to the isotope analyses (Bauer et al., 2016; Bauer and Vennemann, 2014).

$\delta^{18}O$ and δD values of smectite-dominated clays separated from the red boles to approximate the meteoric water composition that prevailed during the Deccan eruptions. $\delta^{18}O$ and δD values of the bole bed clay separates have average values very similar to those previously analzed for similar samples in different localities (Ghosh et al., 2006), although the samples analysed here have a larger range in values, notably during the closing stages of volcanism (towards the top of our profiles). By analogy to Ghosh et al. (2006), it can be concluded that the clay mineral fraction clearly represents weathering products and they are not hydrothermal in origin as previously proposed by Chenet et al., (2008) (Fig. 10). The latter would lead to lower $\delta^{18}O$ values for the clay mineral fraction. Furthermore, the H- and O-isotope composition of two modern soil samples is comparable to that of red boles suggesting a resemblance of the present-day climate in India (arid to semi-arid) comopared to the paleoclimatic conditions existing at the time of red bole formation.

The large variations in both H- and O-isotope values starting from the top of the Bushe Fm until the top of Mahabaleshwhar Fm is surprising though. Compared to the rather homogeneous samples analyzed by Ghosh et al (2006), this may either be related to a higher sampling density and largely different and changing climatic conditions during clay mineral formation or perhaps to different proportions of newly formed clay mineral and a residual, detrital fraction of phyllosilicates in the samples. In the case of rather rapidly changing climatic conditions during the closing stages of Deccan volcanism, lower values of $\delta^{18}O$ and δD would indicate more humid conditions, while higher values could indicate semi-arid conditions. The large variation in isotopic values is certainly not due to analytical errors and may most likely be explained by the concept of 'mock-aridity' (Harris and Van Couvering, 1995) or monsoon like conditions as factors such as temperature variations alone cannot explain the large spread in values at this final stage. Mock aridity describes the effects of volcanism mimic those of semi-aridity (Harris and Vancouvering, 1995) because the formation of large, young basaltic rocks

inhibits the formation of well-developed soils and the growth of vegetation (Harris and Vancouvering, 1995, Font et al, 2020). These climatic variations could also be the result of an acceleration in eruption rate starting at the top of the Bushe Fm (Fig. 11).

5. Conclusion

Based on our multiproxy approach and the detailed geochemical analysis of red boles, we conclude that red boles are formed by weathering of lava flows during periods of volcanic quiescence and consist mainly of clay-rich smectite. The presence of smectite indicates that a semi-arid seasonal climate was prevailing during the formation of bole beds. Changes in weathering indices and also estimates of mean annual precipitation are compatible with a trend of increased chemical weathering in response to increased acid rains towards the top of the Deccan stratigraphy, which also corresponds to an increase in eruption rates towards the top of the Bushe formation. H- and O-isotope compositions are also compatible with average climatic conditions similar to today but with increased intensities of precipitation towards the closing stages of Deccan volcanism. Large changes in clay mineral H- and O-isotope compositions towards the top of the sections could support paleoclimatic instability linked to the paroxysmal mega-pulses of Poladpur, Ambenali and Mahabaleshwhar Fm, with a significant impact on the precipitation pattern due to the accumulation of the 3500 m thick lava pile. Importantly, our results indicate a significant impact of Deccan volcanism on the K-Pg boundary mass extinction thereby suggesting a cause-and-effect relationship.

6. Acknowledgements

We thank T. Monnier and J. C. Lavanchy for their technical assistance in carrying out the different analyses at the University of Lausanne, Switzerland.

7. References

1. Adatte, T., Stinnesbeck, W. and Keller, G., 1996. Lithostratigraphic and mineralogic correlations of near K/T boundary clastic sediments in northeastern Mexico: implications for origin and nature of deposition. *Special Paper of the Geological Society of America*, *307*, pp.211-226.
2. Alvarez, L.W., Alvarez, W., Asaro, F., Michel, H.V., 1980. Extraterrestrial Cause for the Cretaceous-Tertiary Extinction. Science 208, 1095–1108. https://doi.org/10.1126/science.208.4448.1095
3. Babechuk, M.G., Widdowson, M., Kamber, B.S., 2014. Quantifying chemical weathering intensity and trace element release from two contrasting basalt profiles, Deccan Traps, India. Chem Geol 363, 56–75. https://doi.org/10.1016/j.chemgeo.2013.10.027
4. Bauer, K.K., Vennemann, T.W., 2014. Analytical methods for the measurement of hydrogen isotope composition and water content in clay minerals by TC/EA. Chem Geol 363, 229–240. https://doi.org/10.1016/j.chemgeo.2013.10.039
5. Bauer, K.K., Vennemann, T.W., Gilg, H.A., 2016. Stable isotope composition of bentonites from the Swiss and Bavarian Freshwater Molasse as a proxy for paleoprecipitation. Palaeogeogr Palaeoclim Palaeoecol 455, 53–64. https://doi.org/10.1016/j.palaeo.2016.02.002
6. Beane, J.E., Turner, C.A., Hooper, P.R., Subbarao, K.V., Walsh, J.N., 1986. Stratigraphy, composition and form of the Deccan Basalts, Western Ghats, India. B Volcanol 48, 61–83. https://doi.org/10.1007/bf01073513

7. Chenet, A., Fluteau, F., Courtillot, V., Gérard, M., Subbarao, K.V., 2008. Determination of rapid Deccan eruptions across the Cretaceous-Tertiary boundary using paleomagnetic secular variation: Results from a 1200-m-thick section in the Mahabaleshwar escarpment. J Geophys Res Solid Earth 1978 2012 113. https://doi.org/10.1029/2006jb004635
8. Clyde, W.C., Ramezani, J., Johnson, K.R., Bowring, S.A., Jones, M.M., 2016. Direct high-precision U–Pb geochronology of the end-Cretaceous extinction and calibration of Paleocene astronomical timescales. Earth Planet Sc Lett 452, 272–280. https://doi.org/10.1016/j.epsl.2016.07.041
9. Coplen, T.B., 1996. New guidelines for reporting stable hydrogen, carbon, and oxygen isotope-ratio data. Geochim Cosmochim Ac 60, 3359–3360. https://doi.org/10.1016/0016-7037(96)00263-3
10. Courtillot, V., Besse, J., Vandamme, D., Montigny, R., Jaeger, J.-J., Cappetta, H., 1986. Deccan flood basalts at the Cretaceous/Tertiary boundary? Earth Planet Sc Lett 80, 361–374. https://doi.org/10.1016/0012-821x(86)90118-4
11. Courtillot, V., Féraud, G., Maluski, H., Vandamme, D., Moreau, M.G., Besse, J., 1988. Deccan flood basalts and the Cretaceous/Tertiary boundary. Nature 333, 843–846. https://doi.org/10.1038/333843a0
12. Cox, K.G., Hawkesworth, C.J., 1985. Geochemical Stratigraphy of the Deccan Traps at Mahabaleshwar, Western Ghats, India, with Implications for Open System Magmatic Processes. J Petrol 26, 355–377. https://doi.org/10.1093/petrology/26.2.355

13. Duncan, R.A., Pyle, D.G., 1988. Rapid eruption of the Deccan flood basalts at the Cretaceous/Tertiary boundary. Nature 333, 841–843. https://doi.org/10.1038/333841a0
14. E. Font, T. Adatte, A. Abrajevitch, J. Mirão, N. Sharma, V. Sordet, M. Andrade, 2020. Integrated mineralogical and rock magnetic study of Deccan red boles T. Adatte, D.P.G. Bond, G. Keller (Eds.), Mass Extinctions, Volcanism, and Impacts: New Developments: Geol. Soc. Am. Special Paper, vol. 544, pp. 199-222.
15. Eddy, M.P., Schoene, B., Samperton, K.M., Keller, G., Adatte, T., Khadri, S.F.R., 2020. U-Pb zircon age constraints on the earliest eruptions of the Deccan Large Igneous Province, Malwa Plateau, India. Earth Planet Sc Lett 540, 116249. https://doi.org/10.1016/j.epsl.2020.116249
16. Gertsch, B., Keller, G., Adatte, T., Garg, R., Prasad, V., Berner, Z., Fleitmann, D., 2011. Environmental effects of Deccan volcanism across the Cretaceous–Tertiary transition in Meghalaya, India. Earth Planet Sc Lett 310, 272–285. https://doi.org/10.1016/j.epsl.2011.08.015
17. Ghosh, P., Sayeed, M.R.G., Islam, R., Hundekari, S.M., 2006. Inter-basaltic clay (bole bed) horizons from Deccan traps of India: Implications for palaeo-weathering and palaeo-climate during Deccan volcanism. Palaeogeogr Palaeoclim Palaeoecol 242, 90–109. https://doi.org/10.1016/j.palaeo.2006.05.018
18. Harnois, L., 1988. The CIW index: A new chemical index of weathering. Sediment Geol 55, 319–322. https://doi.org/10.1016/0037-0738(88)90137-6

19. Harris, J., Couvering, J.V., 1995. Mock aridity and the paleoecology of volcanically influenced ecosystems. Geology 23, 593–596. https://doi.org/10.1130/0091-7613(1995)023<0593:maatpo>2.3.co;2
20. Hildebrand, A.R., Penfield, G.T., Kring, D.A., Pilkington, M., Z., A.C., Jacobsen, S.B., Boynton, W.V., 1991. Chicxulub Crater: A possible Cretaceous/Tertiary boundary impact crater on the Yucatán Peninsula, Mexico. Geology 19, 867–871. https://doi.org/10.1130/0091-7613(1991)019<0867:ccapct>2.3.co;2.
21. Jay, A.E., Widdowson, M., 2008. Stratigraphy, structure and volcanology of the SE Deccan continental flood basalt province: implications for eruptive extent and volumes. J Geol Soc London 165, 177–188. https://doi.org/10.1144/0016-76492006-062
22. Keller, G., Bhowmick, P.K., Upadhyay, H., Dave, A., Reddy, A.N., Jaiprakash, B.C., Adatte, T., 2011. Deccan volcanism linked to the Cretaceous-Tertiary boundary mass extinction: New evidence from ONGC wells in the Krishna-Godavari Basin. J Geol Soc India 78, 399–428. https://doi.org/10.1007/s12594-011-0107-3
23. Khadri, Syed & Subbarao, K.V. & Hooper, P.R. & Walsh, John. (1988). Stratigraphy of Thakurvadi Formation, Western Deccan Basalt Province, India. Memoirs - Geological Society of India. 10. 281-304.
24. Kirschner, D.L., Sharp, Z.D., 1997. Oxygen isotope analyses of fine-grained minerals and rocks using the laser-extraction technique. Chem Geol 137, 109–115. https://doi.org/10.1016/s0009-2541(96)00123-4

25. Klug, H.P., Alexander, L., 1974. X-ray Diffraction Procedures for Polycrystalline and Amorphous Materials. John Wiley and Sons Inc., New York.
26. Kübler, B., 1983. Dosage quantitatif des minéraux majeurs des roches sédimentaires par diffraction X. Cahier de l'Institut de Géologie de Neuchâtel Série AX N0 1.1 and 12.
27. McLean, D.M., 1985. Deccan traps mantle degassing in the terminal Cretaceous marine extinctions. Cretaceous Res 6, 235–259. https://doi.org/10.1016/0195-6671(85)90048-5
28. Nesbitt, H.W., Young, G.M., 1982. Early Proterozoic climates and plate motions inferred from major element chemistry of lutites. Nature 299, 715–717. https://doi.org/10.1038/299715a0
29. Officer, C.B., Drake, C.L., 1983. The Cretaceous-Tertiary Transition. Science 219, 1383–1390. https://doi.org/10.1126/science.219.4591.1383
30. Olsen, P.E., 1999. Giant Lava Flows, Mass Extinctions, and Mantle Plumes. Science 284, 604–605. https://doi.org/10.1126/science.284.5414.604
31. Pope, K.O., Ocampo, A.C., Duller, C.E., 1991. Mexican site for K/T impact crater? Nature 351, 105–105. https://doi.org/10.1038/351105a0
32. Rampino, M.R., Stothers, R.B., 1988. Flood Basalt Volcanism During the Past 250 Million Years. Science 241, 663–668. https://doi.org/10.1126/science.241.4866.663
33. Schoene, B., Eddy, M.P., Samperton, K.M., Keller, C.B., Keller, G., Adatte, T., Khadri, S.F.R., 2019. U-Pb constraints on pulsed eruption of the Deccan Traps across the end-Cretaceous mass extinction. Science 363, 862–866. https://doi.org/10.1126/science.aau2422

34. Schoene, B., Samperton, K.M., Eddy, M.P., Keller, G., Adatte, T., Bowring, S.A., Khadri, S.F.R., Gertsch, B., 2015. U-Pb geochronology of the Deccan Traps and relation to the end-Cretaceous mass extinction. Science 347, 182–184. https://doi.org/10.1126/science.aaa0118
35. Schulte, P., Alegret, L., Arenillas, I., Arz, J.A., Barton, P.J., Bown, P.R., Bralower, T.J., Christeson, G.L., Claeys, P., Cockell, C.S., Collins, G.S., Deutsch, A., Goldin, T.J., Goto, K., Grajales-Nishimura, J.M., Grieve, R.A.F., Gulick, S.P.S., Johnson, K.R., Kiessling, W., Koeberl, C., Kring, D.A., MacLeod, K.G., Matsui, T., Melosh, J., Montanari, A., Morgan, J.V., Neal, C.R., Nichols, D.J., Norris, R.D., Pierazzo, E., Ravizza, G., Rebolledo-Vieyra, M., Reimold, W.U., Robin, E., Salge, T., Speijer, R.P., Sweet, A.R., Urrutia-Fucugauchi, J., Vajda, V., Whalen, M.T., Willumsen, P.S., 2010. The Chicxulub Asteroid Impact and Mass Extinction at the Cretaceous-Paleogene Boundary. Science 327, 1214–1218. https://doi.org/10.1126/science.1177265
36. Self, S., Jay, A.E., Widdowson, M., Keszthelyi, L.P., 2008. Correlation of the Deccan and Rajahmundry Trap lavas: Are these the longest and largest lava flows on Earth? J Volcanol Geoth Res 172, 3–19. https://doi.org/10.1016/j.jvolgeores.2006.11.012
37. Sepkoski, J.J., 1982. Geological Implications of Impacts of Large Asteroids and Comets on the Earth. Geol Soc Am Spec Pap 283–290. https://doi.org/10.1130/spe190-p283
38. Sepkoski, J.J., 1996. Global Events and Event Stratigraphy in the Phanerozoic, Results of the International Interdisciplinary Cooperation in

the IGCP-Project 216 “Global Biological Events in Earth History” 35–51. https://doi.org/10.1007/978-3-642-79634-0_4

39. Sharp, Z.D., 1990. A laser-based microanalytical method for the in situ determination of oxygen isotope ratios of silicates and oxides. Geochim Cosmochim Ac 54, 1353–1357. https://doi.org/10.1016/0016-7037(90)90160-m
40. Sheldon, N.D., Retallack, G.J., Tanaka, S., 2002. Geochemical Climofunctions from North American Soils and Application to Paleosols across the Eocene-Oligocene Boundary in Oregon. J Geology 110, 687–696. https://doi.org/10.1086/342865
41. Sheldon, N.D., Tabor, N.J., 2009. Quantitative paleoenvironmental and paleoclimatic reconstruction using paleosols. Earth-sci Rev 95, 1–52. https://doi.org/10.1016/j.earscirev.2009.03.004
42. Smit, J., Roep, T.B., Claeys, P., Grajales-Nishimura, J.M. and Bermudez, J., 1996. Coarse-grained, clastic sandstone complex at the K/T boundary around the Gulf of Mexico: Deposition by tsunami waves. *The Cretaceous-Tertiary event and other catastrophes in Earth history*, *307*, p.151.
43. Srivastava, P., Shrivastava, J.P., Sangode, S.J., Srivastava, S., 2016. Weathering characteristics of interflow volcanic boles from Mandla lobe, Eastern Deccan volcanic province. Catena 140, 169–181. https://doi.org/10.1016/j.catena.2016.01.025
44. Stein, R.A., Sheldon, N.D., Allen, S.E., Smith, M.E., Dzombak, R.M., Jicha, B.R., 2021. Climate and ecology in the Rocky Mountain interior after the early Eocene Climatic Optimum. Clim Past 17, 2515–2536. https://doi.org/10.5194/cp-17-2515-2021

45. Vennemann, T.W., Morlok, A., Engelhardt, W. von, Kyser, K., 2001. Stable isotope composition of impact glasses from the Nördlinger Ries impact crater, Germany. Geochim Cosmochim Ac 65, 1325–1336. https://doi.org/10.1016/s0016-7037(00)00600-1
46. Widdowson, M., Walsh, J.N., Subbarao, K.V., 1997. The geochemistry of Indian bole horizons: palaeoenvironmental implications of Deccan intravolcanic palaeosurfaces. Geological Soc Lond Special Publ 120, 269–281. https://doi.org/10.1144/gsl.sp.1997.120.01.17
47. Wignall, P.B., 2001. Large igneous provinces and mass extinctions. Earth-sci Rev 53, 1–33. https://doi.org/10.1016/s0012-8252(00)00037-4

Author contributions

T.A. designed the project and led the research group. N.S. collected the data, interpreted the results, and wrote the manuscript with inputs from T.V., B.S., G.K. and T.A. B.S., G.K., S.K. and T.A. assisted in field data collection. T.V., B.S., G.K., S.K., and T.A. reviewed and provided comments on the manuscript.

Funding

We thank the Swiss National Science Foundation (SNSF grant no. 200020_182017) for supporting this work.

Competing interests

The authors declare no competing interests.

Data availability

All data generated and analysed in this study, including locations of sampling stations have been uploaded to Mendeley Data repository (DOI: 10.17632/s42yx8smb3.1).

Figures

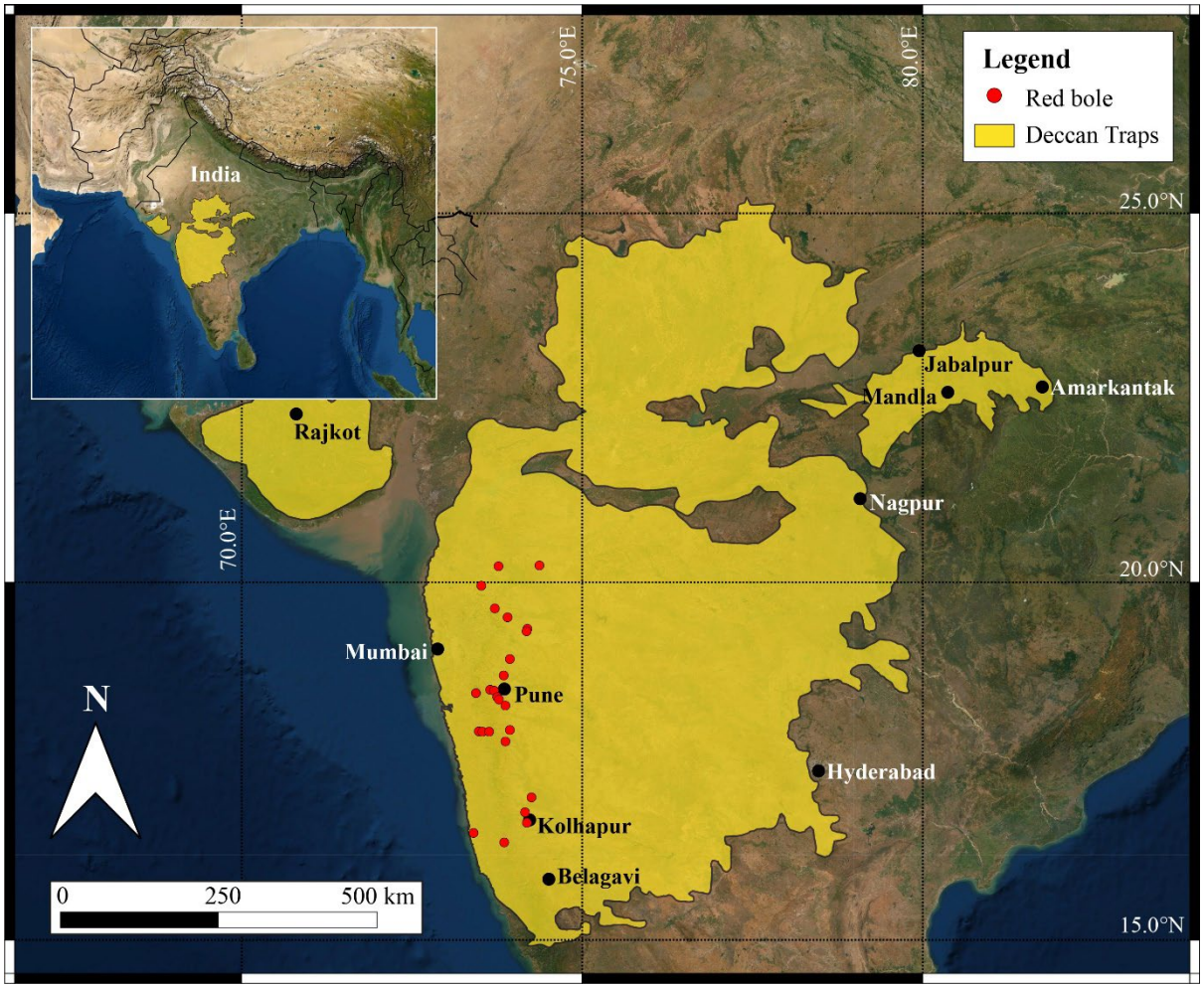

Figure 1

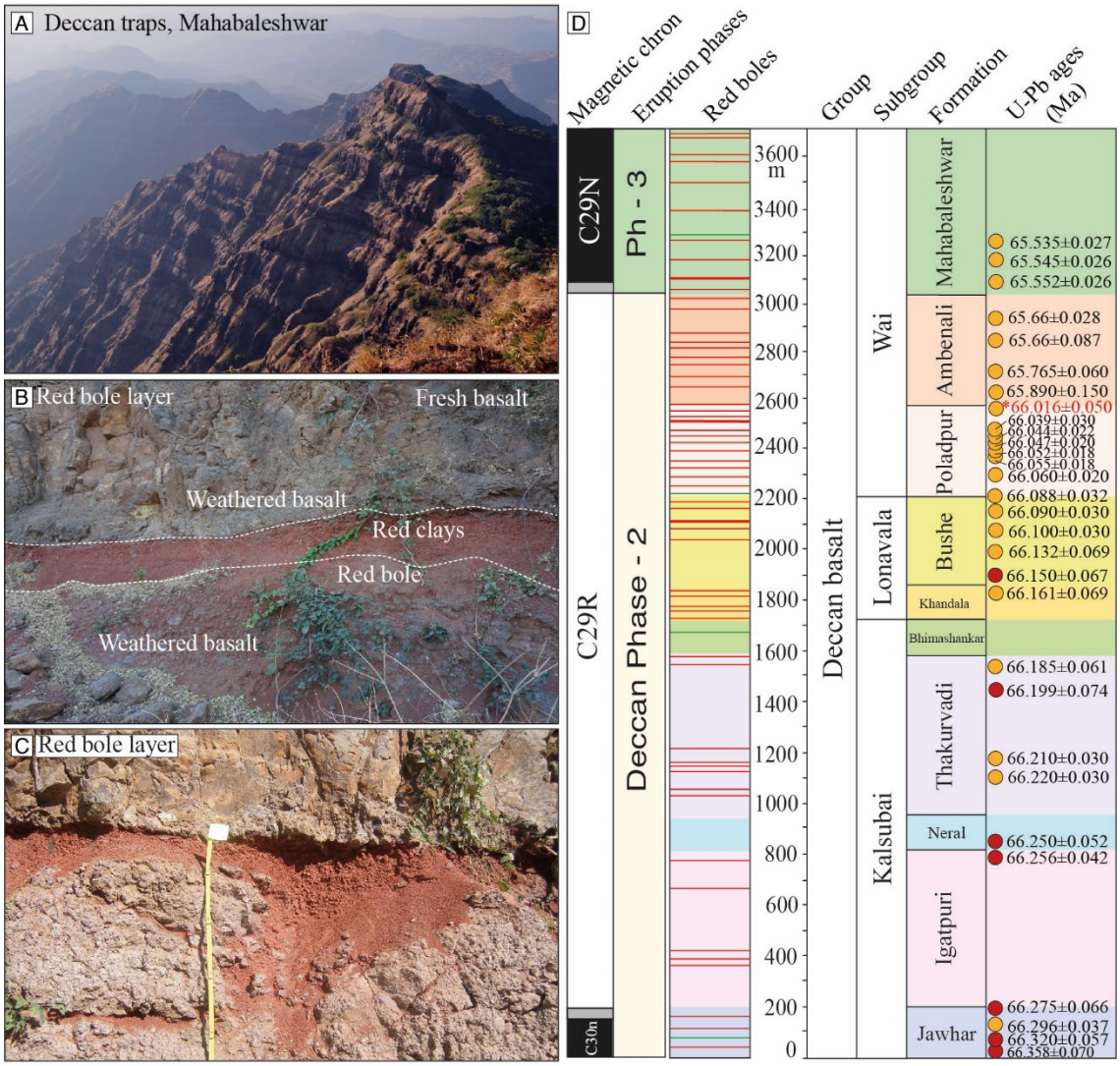
A Deccan traps, Mahabaleshwar
B Red bole layer
Fresh basalt
Weathered basalt
Red clays
Red bole
Weathered basalt
C Red bole layer
D
Magnetic chron
Eruption phases
Red boles
Group
Subgroup
Formation
U-Pb ages (Ma)
C29N
Ph - 3
C29R
Deccan Phase - 2
C30n
3600 m
3400
3200
3000
2800
2600
2400
2200
2000
1800
1600
1400
1200
1000
800
600
400
200
0
Deccan basalt
Wai
Lonavala
Kalsubai
Mahabaleshwar
Ambenali
Poladpur
Bushe
Khandala
Bhimashankar
Thakurvadi
Neral
Igatpuri
Jawhar
65.535±0.027
65.545±0.026
65.552±0.026
65.66±0.028
65.66±0.087
65.765±0.060
65.890±0.150
*66.016±0.050
66.039±0.030
66.044±0.022
66.047±0.020
66.052±0.018
66.055±0.018
66.060±0.020
66.088±0.032
66.090±0.030
66.100±0.030
66.132±0.069
66.150±0.067
66.161±0.069
66.185±0.061
66.199±0.074
66.210±0.030
66.220±0.030
66.250±0.052
66.256±0.042
66.275±0.066
66.296±0.037
66.320±0.057
66.358±0.070

Figure 2

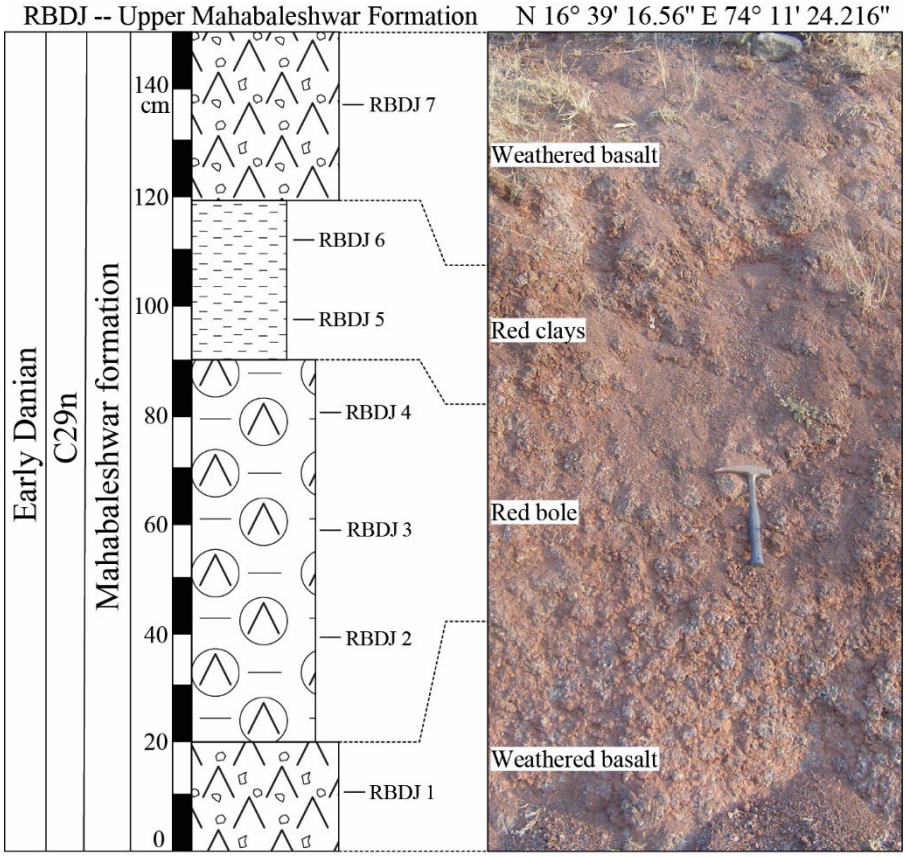
RBDJ -- Upper Mahabaleshwar Formation
N 16° 39' 16.56" E 74° 11' 24.216"
Early Danian
C29n
Mahabaleshwar formation
140 cm
120
100
80
60
40
20
0
RBDJ 7
RBDJ 6
RBDJ 5
RBDJ 4
RBDJ 3
RBDJ 2
RBDJ 1
Weathered basalt
Red clays
Red bole
Weathered basalt

Figure 3

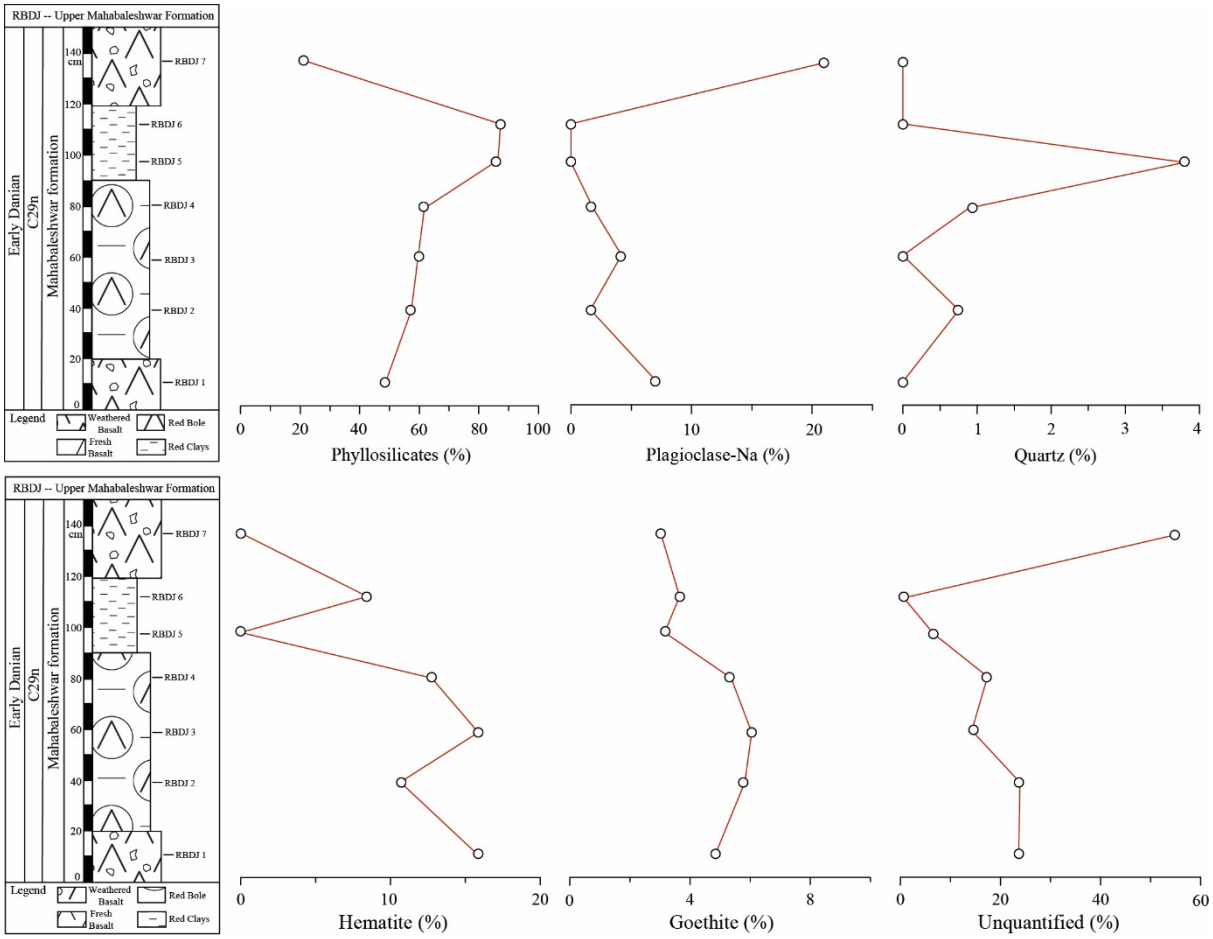
RBDJ -- Upper Mahabaleshwar Formation
Early Danian
C29n
Mahabaleshwar formation
140 cm
120
100
80
60
40
20
0
RBDJ 7
RBDJ 6
RBDJ 5
RBDJ 4
RBDJ 3
RBDJ 2
RBDJ 1
Legend
Weathered Basalt
Fresh Basalt
Red Bole
Red Clays
Phyllosilicates (%)
Plagioclase-Na (%)
Quartz (%)
Hematite (%)
Goethite (%)
Unquantified (%)

Figure 4

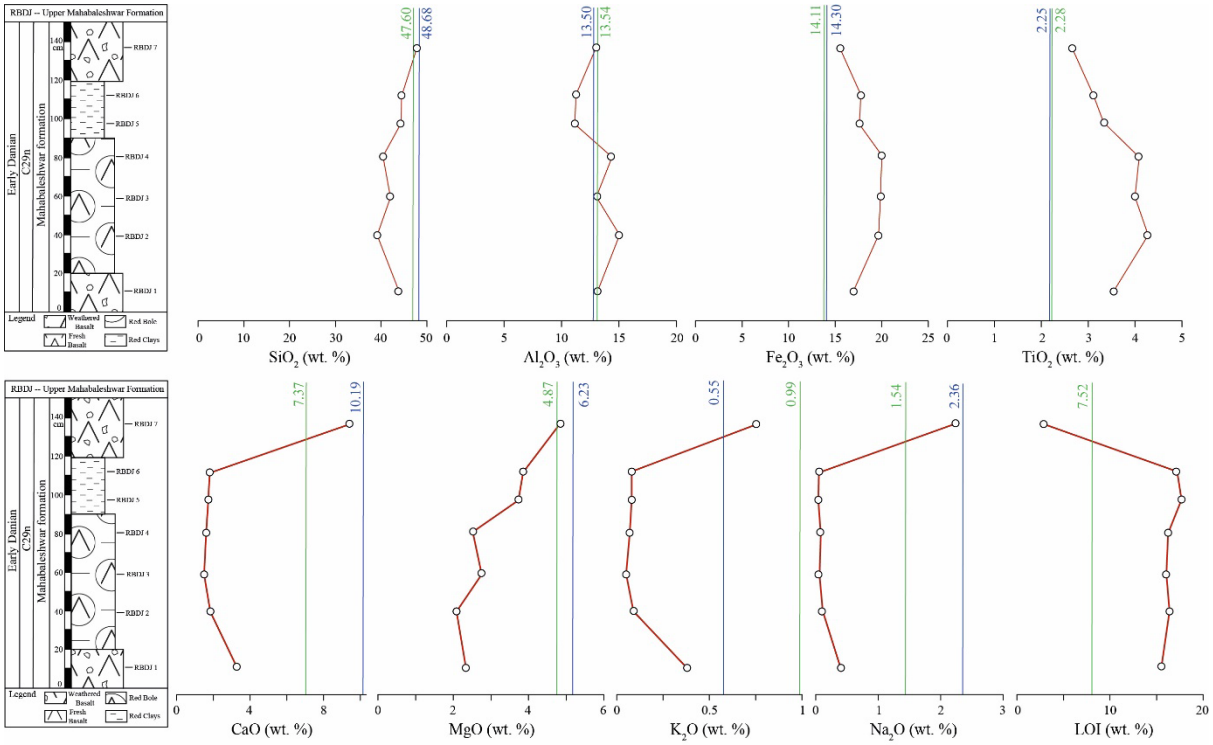

Figure 5

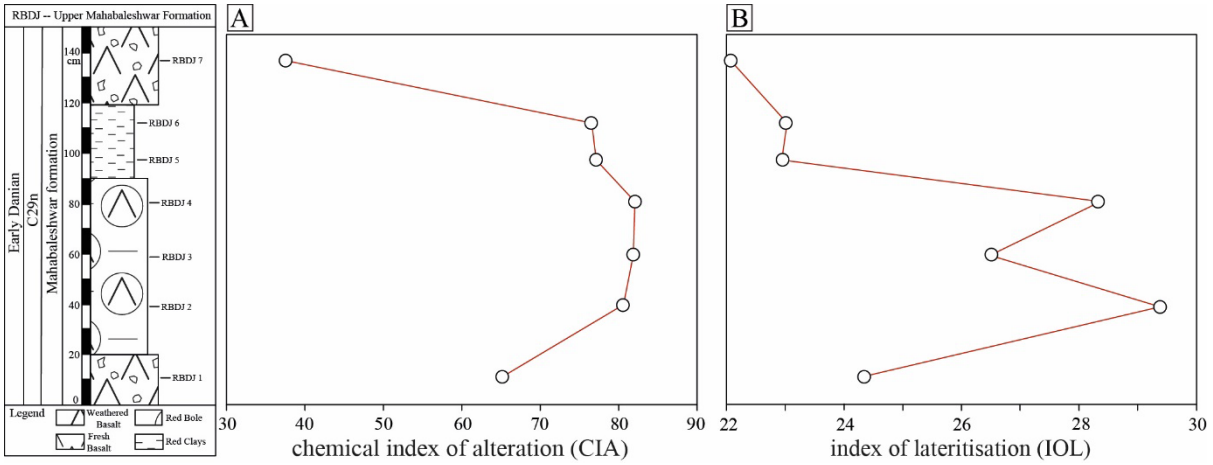

Figure 6

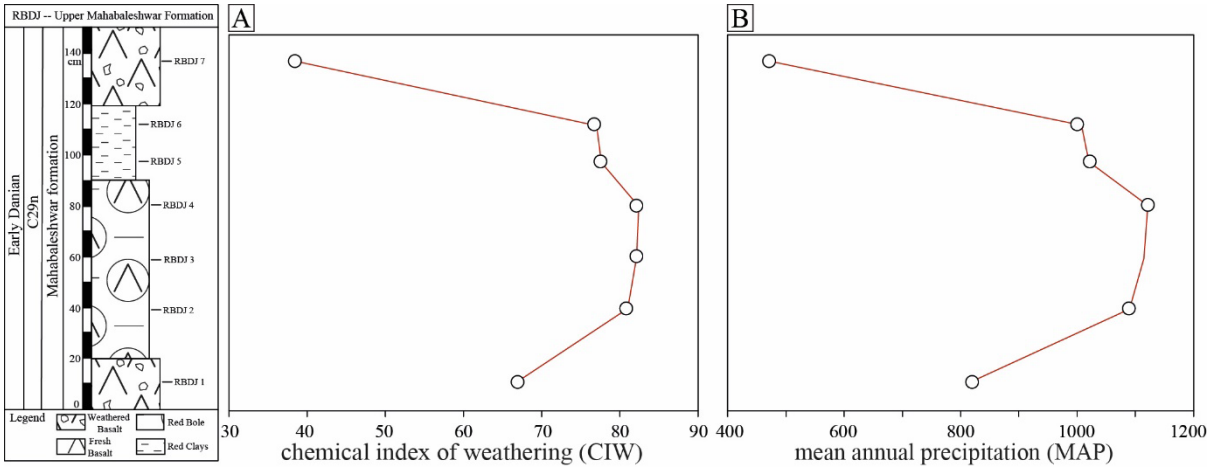

Figure 7

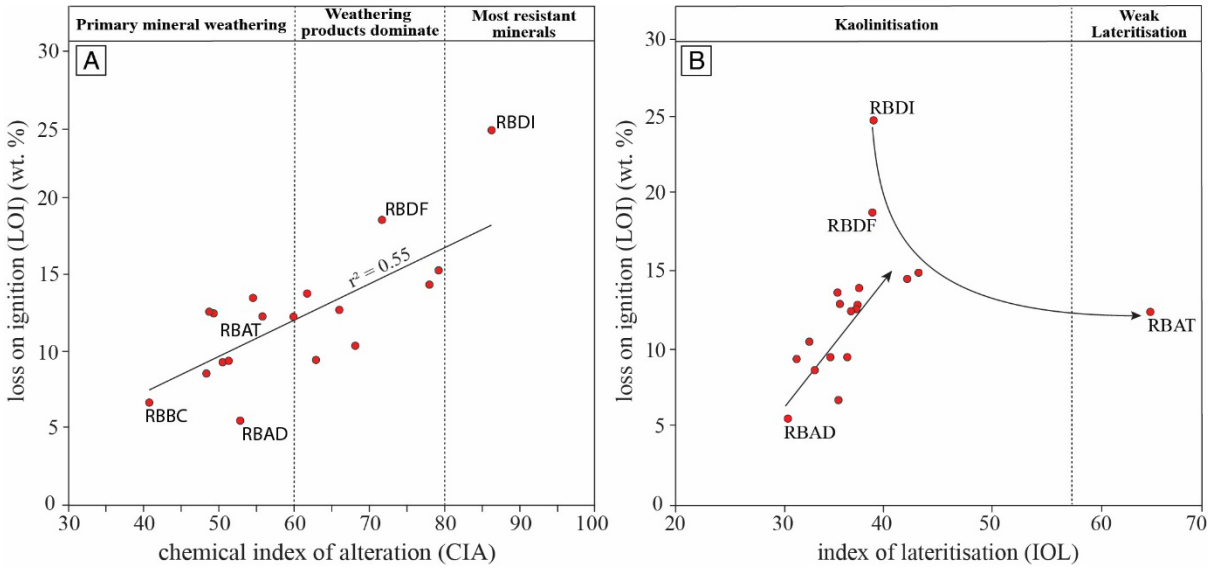

Figure 8

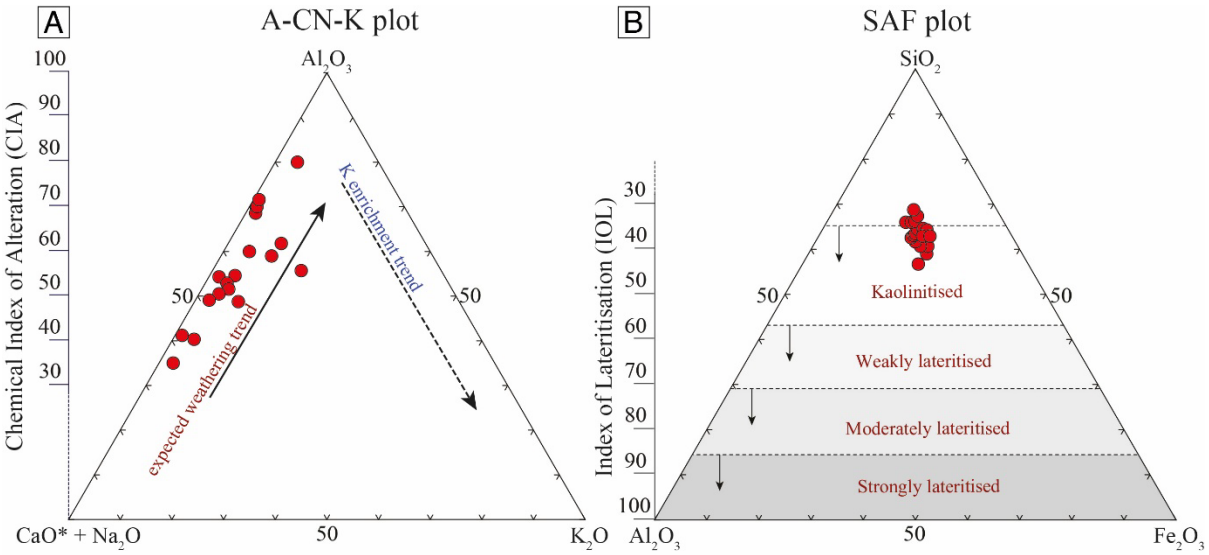

Figure 9

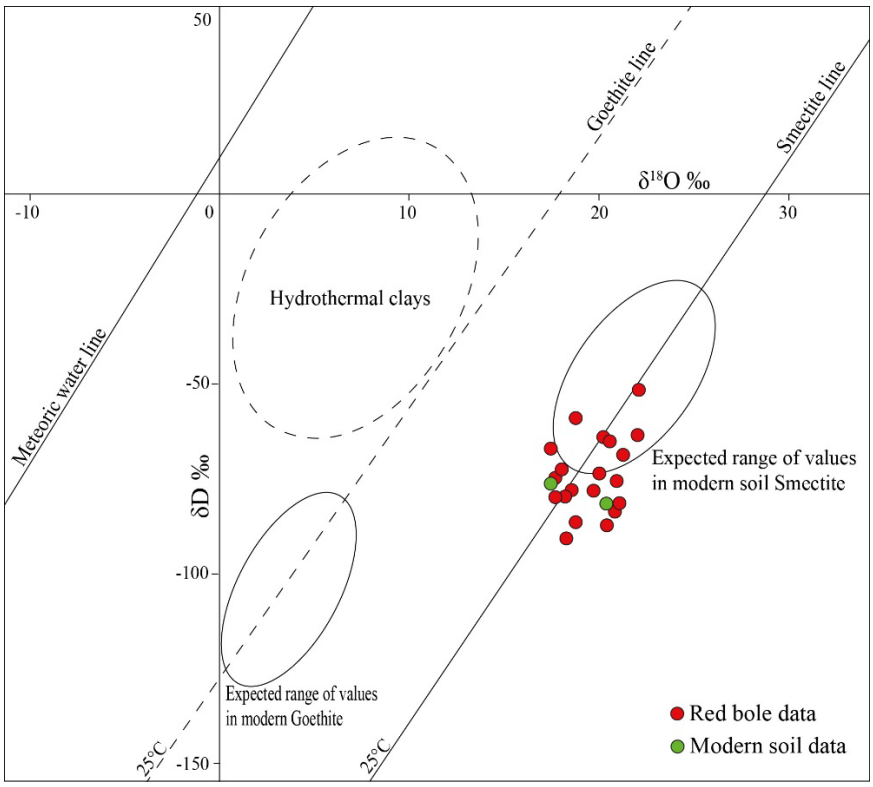

Figure 10

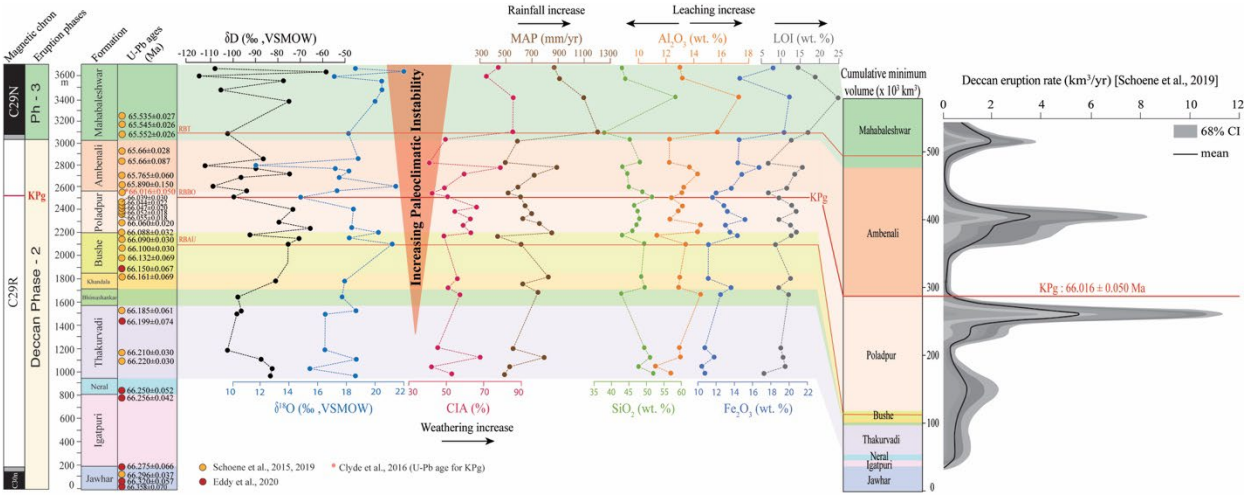

Figure 11

Figure Captions

Figure 1: **The Deccan Volcanic Province**. Map of the Deccan Volcanic Province along with the location of the sampled red bole sections. Figure modified after Srivastava et al., (2016).

Figure 2: **Field images and Deccan stratigraphic formation (A)** View of the Deccan traps from Mahabaleshwar. Individual lava flows can be easily identified as thick basalt layers **(B, C)** a typical red bole section begins with relatively unaltered underlying basalt followed by weathered basalt, friable red clay, a red clay horizon before overlain by the next weathered and relatively unaltered basalt **(C)** Stratigraphy of Deccan basalt group consists of three subgroups namely Kalsubai, Lonavala, and Wai including 10 volcanic formations in total. U-Pb zircon geochronology dates are also indicated to the right (Schoene et al., 2015; Clyde et al., 2016; Schoene et al., 2019; Eddy et al., 2020).

Figure 3: **A typical red bole section.** Section RBDJ sampled in the upper Mahabaleshwar Fm and its different layers which have undergone different degrees of weathering from weathered basalt to red clays.

Figure 4: **Section RBDJ bulk rock mineralogy.** Phyllosilicates constitute up to 90 % of red boles while other major components include sodic plagioclase, quartz, hematite, and goethite. A progressive increase in phyllosilicates in the red boles indicates the gradual increase in weathering from the weathered basalt up to the red clay layer.

Figure 5: **Section RBDJ major elements.** Major elements expressed as Si, Al, Fe, Ti, Ca, Mg, K and Na oxides. Also displayed is the loss on ignition (LOI), which is a measure of the amount (wt. %) of volatiles present. The average relatively unaltered basalt values from this study are shown in green while Deccan basalt mean values from Gertsch et al. (2011) are shown in blue.

Figure 6: **Weathering trends in section RBDJ. (A)** Chemical index of alteration (CIA) increases from the underlying weathered basalt to the red clay layers and progressively decreases in the overlying weathered basalt layer suggesting an increase in weathering towards the middle of the section. **(B)** The index of lateritisation (IOL) values are similar to the CIA values and indicate an increase in weathering in the red bole and red clay layer.

Figure 7: **(A)** Similar to the CIA, the chemical index of weathering (CIW) suggests intense weathering in the red clays **(B).** The red clays also correspond to increased precipitation as inferred from the Mean Annual Precipitation (MAP) estimates.

Figure 8: **Index of lateritisation (IOL) compared with loss on ignition (LOI) and the chemical index of alteration (CIA). (A)** Comparison between IOL and the LOI reflects a change in the LOI when red boles undergo weathering for a longer duration as indicated by the difference in values of red bole RBAT and the RBDI. The upward arrow indicates the increase in LOI with the addition of hydrous clays. **(B)** Comparison between the CIA and LOI with a correlation between the two. Plots modified after Babechuk et al., (2014).

Figure 9: **Weathering trends characterized by the following ternary plots**. (a) A-CN-K ternary plot along the chemical index of alteration (CIA) marks the enrichment trends in aluminum and potassium. (b) SAF ternary plot along index of lateritisation (IOL) estimates. The degree of weathering can be classified from weakly kaolinitised to strongly lateritised.

Figure 10: **Stable isotope cross plot**. δD and $\delta^{18}O$ values of the clay fraction in smectite-rich red bole sections. The results are coherent with values expected for clay formation in soils rather than a hydrothermal, deuteric origin. Figure modified after Ghosh et al. (2006).

Figure 11: **Compilation of red bole data**. The deccan volcanism phase-2 and 3 stratigraphy and U-Pb ages of available red boles are reported with their respective stable isotope values, weathering index CIA, mean annual precipitation (MAP), and oxides of different elements. Our data suggests increased paleoclimatic instability towards the KPg boundary and in the paroxysmal Deccan phases corresponding to the Poladpur, Ambenali and Mahabaleshwhar Fms. Increased weathering and precipitation rates are observed in the same interval, which includes the KPg boundary and coincide with an increase in leaching of immobile oxides of Al, Fe and Si.